Towards the influences of the d-resonance splitting on the electronic density of states of an amorphous transition metal

1992 J. Phys.: Condens. Matter 4 4441

(http://iopscience.iop.org/0953-8984/4/18/011)

J. Phys.: Condens. Matter 4 (1992) 4441–4457. Printed in the UK

Towards the influence of the d-resonance splitting on the electronic density of states of an amorphous transition metal

Heinrich Solbrig and Michael Schubert
Technical University Chemnitz, Institute of Theoretical Physics, PO Box 964, O-9010 Chemnitz, Federal Republic of Germany

Received 12 February 1991, in final form 19 December 1991

Abstract. Electronic multiple scattering in close pairs of effective atoms splits the d-resonance of the bare effective atom into a doublet of resonances with different axial symmetries. The modifications of the bare atomic sphere electronic density of states, due to the first two neighbour shells, are analysed in terms of this d-resonance splitting. Employing pure amorphous Fe as a model we show that the radial distribution of very close neighbours is the dominant structure property at the upper d-band edge. Long-range multiple scattering blurs both the lower d-band edge and the lower component of the resonance doublet. Neighbours in the dip of the second pair correlation shell are found to occupy energetically disadvantageous positions which should give rise to corresponding contributions to the effective interatomic force due to the d-resonance splitting.

1. Introduction

Two questions relating to amorphous metals are considered in depth: (i) What influence has the residual short-range order on the electronic density of states? (ii) How can amorphous structures be described, and which effective interatomic forces provide realistic models upon simulated quenching? The present paper concentrates on Fe atoms in Fe-rich amorphous phases, employing a model of non-magnetic pure amorphous Fe. It will be shown that electronic multiple scattering in a pair of effective Fe atoms provides links between the electronic density of states on the one hand and the real-space structure on the other.

Our material modelling is straightforward: structure models are obtained employing molecular dynamics and the Metropolis Monte Carlo method, both with Morse-type effective atom–atom interaction. The local electronic density of states (LDOS) is calculated by means of a non-self-consistent muffin-tin (MT) scattered-wave concept. It starts from extended electron states and is thus complementary to predominant approaches that are based on the atomic orbitals (e.g. the recursion method, Haydock *et al* 1972, 1975). Despite being less qualified for rapid computational implementation, such attempts can be considered as real in the physical sense, because they deal with effective atoms in the superposition potential (Mattheiss 1964). Hence, from the very beginning, contributions beyond the two-centre terms are included. Obviously, the d-resonance of the MT scatterers of transition metals is a consequence of this approach.

One question which belongs to the first research topic mentioned above is that of the number of peaks in the LDOS of Fe-rich amorphous phases. Photoemission spectra of

thin polycrystalline BCC-Fe films show a main peak slightly below the Fermi energy and a second weak feature at more than 2 eV binding energy (Pessa *et al* 1976, Paul and Neddermeyer 1985, Ley *et al* 1977), in agreement with theoretical results (Singh *et al* 1975). In the photoemission data from amorphous phases with about 80 at.% Fe however, the lower peak can hardly be found (Paul and Neddermeyer 1985).

With respect to the appearance of a second peak, theoretical results are ambiguous. A trend towards a split d-band is found in recursion calculations upon including the Fe 4p atomic orbitals in addition to the 3d and 4s orbitals (Varga and Krempasky 1989, Varga 1990, Krajči and Mrafko 1988). Fujiwara (1984) in a self-consistent linear MT orbital method, obtained a pronounced lower peak. This peak was not extinguished by the achieved degree of local self-consistency. Its reduction to the level observed in experiments is a matter of sd-hybridization and requires long-range multiple scattering (MS) of s-waves to be taken into account (H–NFE–TB approach for crystalline transition metals, Ziman 1965, Heine 1967). We will show that MS in a pair of effective Fe atoms explains both the formation of a resonance doublet and the preferential decay of its lower component.

Established diffraction methods show the second pair correlation shell (SPCS) of amorphous metals typically split into two subshells (Nold *et al* 1981, Ichikawa 1973). It is a goal of the second research topic mentioned above to obtain this splitting by modelling the atomic dynamics which occur during the production of the material. There are also successful attempts reviewed by Cargill (1975) to construct static structure models where geometric construction principles (Bennett 1972) replace the forces really acting. Thus, repulsive forces between atoms in contact are considered by the hard-sphere model.

A second principle comprises prescriptions which achieve a space-filling addition of new atoms starting from a seed. Thus, they have similar consequences as attractive forces between atoms which are not in contact. It turns out (Cargill 1975) that distinct splittings of the SPCS occur for particularly dense-packed clusters (Ichikawa 1973, Sadoc *et al* 1973). Such clusters must be carefully prepared with respect to the second construction principle. We conclude that the splitting is facilitated by attractive forces which urge the atoms of the inner side of the SPCS to occupy free hollow-sites on the outer side of the first pair correlation shell (FPCS). In the pair correlation function, however, from these dynamics, a distinct splitting can arise only if the atoms of the first shell behave like a sufficiently flat ground, i.e. coordination close to twelve with almost identical distances from the central atom. Obviously, the common quenching techniques (Hilsch 1960, Jones 1973) promote the local relaxation towards such compact configurations of 13 atoms. Thus, high contents of nearly icosahedral first-neighbour shells were obtained by the simulation of supercooled liquids (Steinhardt *et al* 1983) and simple-metal glasses (Hafner 1988). The binding energy of small Fe clusters (Harris and McMaster 1986) indicates FCC-like arrangements to be also probable results of the local relaxation. Surface contributions, however, act in a less predictable way.

Most computer simulations of amorphous transition metals employ effective interatomic potentials which are steeply truncated between the first two neighbour shells and thus facilitate the second construction principle (truncated Morse potentials, Fujiwara and Ishii 1980). We focus here on the possible contributions to the effective interatomic potential, which are due to the effective atom d-resonance splitting. This is beyond present concepts (Hausleitner *et al* 1991). It will turn out that electronic MS in a pair of effective Fe atoms supports the guess for attractive forces to act also in the dip of the SPCS. This concept will be tested in our structure modelling upon truncating the Morse potential just between the two subpeaks of the SPCS.

The paper is organized as follows: The employed MT scattered-wave approach is outlined in section 2. Results of the structure simulation are presented in section 3. In section 4 we develop the concept of resonance splitting which is then applied in section 5 to the splitting of the SPCS. Finally, section 6 deals with the influence which the radial distribution of neighbours has on the LDOS.

2. Electronic density of states

The real-space representation of the Green function (GF) is the starting point for the calculation of the LDOS. Commonly, MS approaches to the GF are derived from the formal scattering theory (Gonis *et al* 1989) where the scattering-path operator (SPO), $\tau_{sL,s'L'}$ (Györffy and Stott 1971), is the most important concept.

Including all scattering paths, this two-site matrix transforms the incident-field amplitudes of a first atomic scattering event at the site $\boldsymbol{R}_{s'}$, into the outgoing-field amplitudes of a final atomic scattering event at the site $\boldsymbol{R}_s$. For the calculation of the LDOS of an atomic sphere, however, only the site-diagonal GF is needed. In the following, we outline an approach to the LDOS (Solbrig 1987) that is strictly confined to one-site arguments. Rather than a formal scattering theory, the view of electron diffraction is a guideline.

2.1. Multiple scattering in muffin-tin systems

Consider an electron of energy $E = k^2$ in a liquid or amorphous metal. We adopt an MT model where the effective atoms are described by non-overlapping spherical scatterers in the vacuum. Hence, eigenfunctions of the angular momentum $L = (l, m)$ are suitable basis sets (see the appendix). In a spherical vacuum shell around the MT at $\boldsymbol{R}_s$, the electron wave function can be decomposed into regular vacuum waves $j_L(\boldsymbol{r})$ ('incident fields', amplitudes Φ_{sL}) and singular outgoing vacuum waves $h_L^{(1)}(\boldsymbol{r})$ ('scattered fields', amplitudes $\mathrm{i}kf_{sl}\,\Phi_{sL}$, $f_{sl} = \exp(\mathrm{i}\delta_{sl})\sin\delta_{sl}/k$ partial scattering amplitudes, $\delta_{sl}(E)$ partial scattering phase shifts). The incident field amplitude Φ_{sL} consists of scattered fields emerging from the other atoms at $\boldsymbol{R}_{s'}$ and a possible contribution Φ_{sL}^{P} ('primary field') of a particle source. This is the physical content of the basic equations of MS,

$$\Phi_{sL} = \Phi_{sL}^{\mathrm{P}} + \sum_{s'L'} C_{sL,s'L'}\Phi_{s'L'}. \tag{1}$$

The scattering-propagation matrix,

$$C_{sL,s'L'} = G_{sL,s'L'}\,\mathrm{i}kf_{s'l'} \tag{2}$$

describes scattering at the site $\boldsymbol{R}_{s'}$ followed by vacuum-wave propagation to the site $\boldsymbol{R}_s$ where

$$G_{sL,s'L'} = (1-\delta_{ss'})\sum_{\bar{L}} h_{\bar{L}}^{(1)}(\boldsymbol{R}_{ss'})\sqrt{4\pi}\int \mathrm{d}\Omega\, Y_L Y_{\bar{L}} Y_{L'}^{*} \tag{3}$$

are the structure constants ($\boldsymbol{R}_{ss'} \equiv \boldsymbol{R}_s - \boldsymbol{R}_{s'}$, Y_L spherical harmonics, see the appendix). The formal MS theory employs the single-site transition matrix $t_{sL,s'L'} = -f_{sl}\delta_{ss'}\delta_{LL'}$ in connection with structure constants $\bar{G}_{sL,s'L'} = -\mathrm{i}kG_{sL,s'L'}$ which does not alter the matrix C (2).

In the following, we adopt a compact notation in the linear vector space spread by the atomic scattering channels $|sL\rangle$. Upon defining vectors,

$$|\Phi\rangle = \sum_{sL}\Phi_{sL}|sL\rangle \qquad |\Phi^{\mathrm{P}}\rangle = \sum_{sL}\Phi_{sL}^{\mathrm{P}}|sL\rangle \tag{4}$$

we find for the basic equations (1)

$$|\Phi\rangle = |\Phi^{\mathrm{P}}\rangle + C|\Phi\rangle \tag{1a}$$

where

$$|\Phi\rangle = (I - C)^{-1}|\Phi^{\mathrm{p}}\rangle \tag{5}$$

is the formal solution of (1*a*). Note that, except for the final scattering, (5) performs just the transition which was ascribed above to the SPO. With $|\Phi^{\mathrm{p}}\rangle = |s'L'\rangle$ we obtain the SPO upon adding this final scattering: $\tau_{sL,s'L'} = \mathrm{i}kf_{sl}\langle sL|(I - C)^{-1}|s'L'\rangle$. But for comparison with the SPO $\bar{\tau}$ as employed by Gonis *et al* (1989), a factor $-\mathrm{i}k$ has to be joined with the singular outgoing vacuum waves. This provides in agreement with Gonis *et al* (1989)

$$\bar{\tau}_{sL,s'L'} = -f_{sl}\langle sL|(I - C)^{-1}|s'L'\rangle = [(t^{-1} - \bar{G})^{-1}]_{sL,s'L'}. \tag{6}$$

Rather than the whole vector $|\Phi\rangle$, solving physical problems requires only projections $\langle\Phi^{\mathrm{f}}|\Phi\rangle$ on certain final vectors $|\Phi^{\mathrm{f}}\rangle$. Common diffraction problems are thus specified by plane waves for both $|\Phi^{\mathrm{f}}\rangle$ and $|\Phi^{\mathrm{p}}\rangle$. It turns out that the LDOS involves a diffraction problem where the considered atomic sphere plays a three-fold part: emitter of the primary field, part of the scatterer ensemble, and detector of the back-scattered field.

2.2. *Green function and local electronic density of states*

The LDOS of the atomic sphere at $\boldsymbol{R}_s$ (ASs) can be calculated from the outgoing wave GF according to

$$D_s(E) = -\frac{2}{\pi}\int_{\mathrm{ASs}} \mathrm{d}^3r\, \mathrm{Im}\, G_s^+(\boldsymbol{r}, \boldsymbol{r}, E). \tag{7}$$

Upon generalizing the bare-MT GF to include the actual environment of the ASs one obtains

$$G_s^+(\boldsymbol{r}, \boldsymbol{r}', k^2) = \frac{-\mathrm{i}k}{4\pi}\sum_L [H_{sL}^+(r_>) + \sum_{L'} J_{sL'}(r_>)T_{sL'L}]J_{sL}(r_<)^* \tag{8}$$

where the basic solutions of the MT potential, J_{sL} and H_{sL}^+, are defined in the appendix. This generalization comprises all regular waves $J_{sL'}$ $T_{sL'L}$ in the ASs which arise from inward back-scattering of an outgoing singular wave H_{sL}^+ of unit amplitude. The $T_{sL'L}$ are thus the elements of the MT-wave reflection matrix which characterizes the environment of the ASs.

The $T_{sL'L}$ define reflection processes in terms of MT waves which can be reformulated in terms of vacuum waves, j_L and $h_L^{(1)}$: in a vacuum shell around the MT at $\boldsymbol{R}_s$ we have $H_{sL}^+ = \exp(\mathrm{i}\delta_{sl})h_L^{(1)}$ (see the appendix). Hence, the emission of an MT wave H_{sL}^+ with unit amplitude produces a primary field $|\Phi^{\mathrm{p}}\rangle = \exp(\mathrm{i}\delta_{sl})C|sL\rangle/\mathrm{i}kf_{sl}$ which acts on all the other atoms. After MS, $|\Phi\rangle = (I - C)^{-1}C|sL\rangle \exp(\mathrm{i}\delta_{sl})/\mathrm{i}kf_{sl}$ (5) will be the vector of the incident field. The step back to amplitudes of MT waves, J_{sL}, is performed by means of the representation $J_{sL} = \exp(-\mathrm{i}\delta_{sl})(j_L + \mathrm{i}kf_{sl}h_L^{(1)})$ in a vacuum shell round the MT at $\boldsymbol{R}_s$ (see the appendix). One obtains $T_{sL'L} = \exp(\mathrm{i}\delta_{sl'})\langle sL'|\Phi\rangle$. Hence, the MT-wave reflection matrix is derived from MS of vacuum waves by the formula

$$T_{sL'L} = \exp(\mathrm{i}\delta_{sl'})\langle sL'|(I - C)^{-1}C|sL\rangle \exp(\mathrm{i}\delta_{sl})/\mathrm{i}kf_{sl}. \tag{9}$$

For comparison with Gonis *et al* (1989) we introduce the SPO τ (6). The result,

$$-\mathrm{i}k\, T_{sL'L} = \exp(\mathrm{i}\delta_{sl'})[t^{-1}(\bar{\tau} - t)t^{-1}]_{sL',sL} \exp(\mathrm{i}\delta_{sl}) \tag{10}$$

shows that the SPO comprises the scattering by the ASs itself which must be removed

afterwards. With respect to the basis functions employed in the GF (8), the MT-wave reflection matrix $T_{sL'L}$ characterizes the environment more directly than the SPO. Our basis set is chosen so as to provide the intended representation (11) of the LDOS. The choice taken by Gonis *et al* (1989) makes the SPO the preferable information quantity.

Upon integrating the LDOS (7) with (8) one obtains the angular momentum decomposition of the LDOS,

$$D_s(E) = \sum_l D_{sl}(E) = \sum_l D^0_{sl}(E)\left(1 + \mathrm{Re}\,\frac{1}{2l+1}\sum_m T_{sLL}\right). \tag{11}$$

Here, the partial LDOS of the embedded ASS, D_{sl}, is derived from that of the bare ASS, $D^0_{sl}(E)$ (see the appendix), and the environment correction, $\mathrm{Re}\,\Sigma_m T_{sLL}/(2l+1)$. In a certain sense, the ASS performs, employing its own eigenfunctions, an angular momentum sensitive structure analysis of its environment: MT waves are emitted with $L = (l,-l),\ldots,(l,l)$, and the L-diagonal back-scattering is received from the environment. Equation (9) tells us what this looks like in terms of vacuum waves where the ASS itself is a perturbation of the homogeneous space and thus participates in the MS.

The LDOS (11) is derived by (9) from all scattering-path cycles which start and terminate at the channel $|sL\rangle$.

$$T_{sLL} = \sum_{\text{cycles}} T^{\text{cyc}}_{sLL}. \tag{12}$$

According to (11), cycles with $\arg T^{\text{cyc}}_{sLL} \approx 0\,(\pi)$ set a trend towards increasing (decreasing) partial LDOS. They will be referred to as constructive (destructive) cycles. Indifferent cycles ($|\arg T^{\text{cyc}}_{sLL}| \approx \pi/2$) have no influence on the LDOS.

2.3. Numerical implementation

The calculation of T_{sLL} (9) can be seen in the context of (1*a*): solve for $(I-C)|\Phi\rangle = C|sL\rangle/ikf_{sl}$ and then take $\exp(i2\delta_{sl})\langle sL|\Phi\rangle$. This makes Gaussian elimination highly suitable. Because, if the channel $|sL\rangle$ is arranged as to be the last one in the sequence, the elimination procedure can be confined to a triangle matrix. It is the advantage of this numerical technique that many MS problems, each with its own vector $|\Phi^p\rangle$ in (1*a*), can be solved simultaneously without mixing them. Then, the processing of the matrix $(I-C)$ is extended beyond the triangle state. This is particularly valuable if the LDOS per atom is aimed at.

On the other hand, our task can be seen in the context of the recursion method for calculating matrix elements of the Green function (Haydock *et al* 1972, 1975). In the standard case where the Hamiltonian is Hermitian a one-sided recursion provides the diagonal elements. Two-sided recursion schemes are needed, however, if the Hamiltonian is non-Hermitian (Haydock and Kelly 1975) and for non-diagonal elements (Nex 1978, Ballentine and Kolář 1986). As demonstrated by Solbrig (1987), the two-sided recursion method for diagonal elements (Haydock and Kelly 1975) can be applied to the present MS problem. Hence, simple analysis based on the three-diagonal representation of C (2) provides the continuous fraction

$$\langle sL|(I-C)^{-1}C|sL\rangle = \cfrac{1}{1 - C_{00} - \cfrac{C_{01}C_{10}}{1 - C_{11} - \cfrac{C_{12}C_{21}}{1 - C_{22} - \ldots}}} - 1 \tag{13}$$

where $C_{n\pm1,n} = \langle v_{n\pm1}|C|u_n\rangle$ describes the transition from the incident field distribution

$|u_n\rangle$ to the neighbouring $|u_{n\pm1}\rangle$ by scattering. MS is thus interpreted as including step by step the more and more remote elements $|u_n\rangle$ of a hierarchy of incident-field 'patterns'.

With one exception, all subsequent calculations are performed by means of the Gaussian elimination. Scattering recursion is the method of choice only if information from certain levels of the recursion process is required. This will be noticed explicitly.

3. Structure models

This paper deals with structure modelling for two reasons: (i) we intend to demonstrate that a distinct splitting of the SPCS is maintained against thermal fluctuations at 300 K even if the enhanced interatomic attraction is located in the dip of the SPCS; (ii) for the calculation of the LDOS we need a cluster which represents structure in the thermal equilibrium.

3.1. Simulation of the thermal equilibrium

As shown by Milstein (1973), a Morse-type atom–atom interaction can well account for the elastic properties of cubic metals. Fujiwara and Ishii (1980) describe amorphous Fe–P phases upon terminating the Morse potential at the minimum r_0 and then replacing it by a smooth truncation function up to $1.4\,r_0$. Hence, the attractive branch of the force is strengthened, but at the same time it is confined to neighbours which belong to the inner side of the SPCS. These are just the kind of forces which support a space-filling coordination of atoms (cf the second construction principle, and the introduction). A steep potential rise between the first two-neighbour shells is also obtained by first-principle calculations (amorphous simple metals, pseudo-potential approach, Hafner and Jaswal 1988; liquid transition metals, H–NFE–TB, Hauseleitner *et al* 1991). But, rather than a cut-off, first-principle potentials exhibit at least a weak medium-range oscillation which is important with respect to the stability of amorphous metals (Häussler 1991). Li and Cowlam (1990) derive strongly oscillating potentials from measured partial structure factors of $Fe_{80}B_{20}$.

We conclude that, within the limits set by the present poor characterization of amorphous structures, several effective interatomic potentials provide satisfactory results. With respect to Morse-derived potentials, we will show that the truncation range can be moved to larger distances. Instead of $r_0 \rightarrow 1.4\,r_0$ as employed by Fujiwara and Ishii (1980) we take $1.60\,r_0 \rightarrow 1.87\,r_0$. Additional attractive forces are thus located just in the dip of the SPCS. In section 5 we will show that good reasons can be given for an extended attractive range. Our effective potential reads as

$$V(r) = D[\exp(-2a(r/r_0 - 1)) - 2\exp(-a(r/r_0 - 1))]F(r/r_0) \qquad (14a)$$

where

$$F(r/r_0) = \begin{cases} 1 \\ \exp(-\alpha(r - r_t)/r_0) \\ 0 \end{cases} \quad \text{for} \begin{cases} r < r_t \\ r_t \leq r \leq r_c \\ r_c < r \end{cases} \qquad (14b)$$

is the truncation function. The following parameters are adopted: 256 atoms with periodic boundary conditions, density $0.012\,165\ \text{au}^{-3}$ (Fujiwara 1979) which corresponds to $7.61\ \text{g cm}^{-3}$, temperature 300 K, $D = 0.03749$ au (Fujiwara and Ishii 1980),

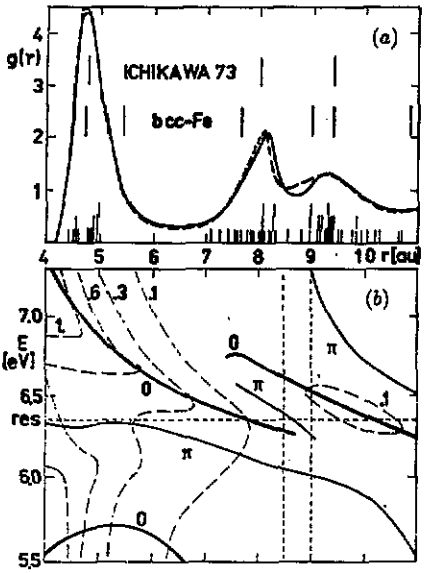

Figure 1. (*a*) Pair correlation function $g(r)$ sampled from 50 instantaneous configurations of the 256-atom cluster along an equilibrium trajectory; full curve—molecular dynamics, broken curve—Monte Carlo; lowest bars—sequence of neighbours in a typical member of the group ICSYS (the cluster ICOCL). Other bars indicate the observed peak positions of a-Fe (Ichikawa 1973) and the neighbours in BCC-Fe. (*b*) Contour maps of the one-neighbour environment correction T_2 (19); full lines—arg T_2; broken lines—$|T_2|$; res—energy of the atomic d-resonance. Electronic d-states are piled up (removed) for arg $T_2 \approx 0$ (π).

$a = 4$, $r_0 = 5.05$ au (Krajči 1987), $\alpha = 12.5$ and $r_t = 8.10$ au as well as $r_c = 9.45$ au close to the observed peak positions (Ichikawa 1973).

Starting from a distribution of hard spheres at 6000 K, equilibrium trajectories were generated for 300 K by means of molecular dynamics (microcanonical ensemble, Verlet algorithm (Verlet 1967), time step 2×10^{-14} s) and by the Metropolis Monte Carlo method. Upon averaging over 50 instantaneous configurations along an equilibrium trajectory, we obtain pair correlation functions with a distinct splitting of the SPCS (figure 1(*a*)). Apart from minor deviations, the subpeaks in figure 1(*a*) have the positions as reported by Ichikawa (1973) for thin amorphous Fe films which are deposited at the temperature of liquid He. The splitting must be due to the additional inward-pointing forces in the dip of the SPCS, which are introduced by the truncation (14*b*). For proof we have replaced the truncation function by a cut-off at 12 au which subjects all second neighbours to the bare Morse potential. Then, no splitting is obtained on the average along equilibrium trajectories at 300 K.

3.2. The structure of the nearest-neighbour shell

We take one instantaneous configuration of the 256 atoms, which has a distribution of the pair distances close to the average along the equilibrium trajectory. Each atom is characterized with respect to the arrangement of its first twelve neighbours. The radial distribution is described by the average distance, $\bar{r}(12)$, and by the mean square deviation of the distances, $\overline{\Delta r}(12)$. Figure 2(*a*) shows the 256 atoms in the $\bar{r} - \overline{\Delta r}$ plane. Besides a majority of less peculiar systems there are very compact shells (ICSYS). It turns out that all members of the group ICSYS have nearly icosahedral structures. As shown in figure 1(*a*) and recently reported by Watanabe and Tsumuraya (1990), in particular around almost icosahedral 13-atom clusters, the population at distances which belong to the dip of the SPCS is drastically reduced. Such findings confirm the guess that compact first neighbour shells with a small $\overline{\Delta r}(12)$ facilitate the appearance of a distinct splitting.

The angular arrangement of the first twelve neighbours can be characterized by the 66 bond angles. Figure 2(*b*) shows the average bond-angle distribution of the 256 atoms.

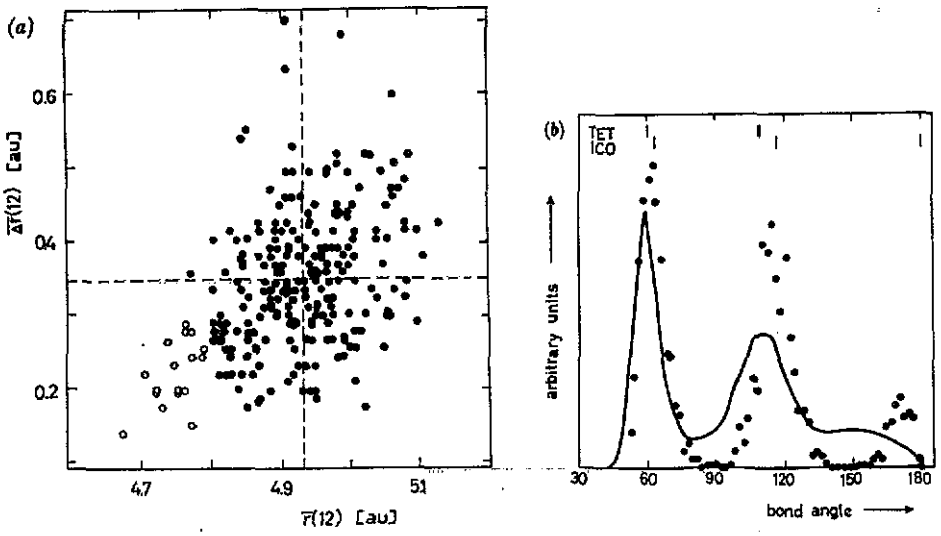

Figure 2. (*a*) Radial distribution of the first twelve neighbours in the 256-atom cluster; $\bar{r}(12)$ is the average distance; $\overline{\Delta r}(12)$ is the mean square deviation of distances; broken lines—ensemble averages, open circles—nearly icosahedral 13-atom clusters (the group ICSYS); (*b*) Distribution of the bond angles θ to the twelve first neighbours in the 256-atom cluster; full curve—ensemble average; full circles—average of the group ICSYS; ICO—icosahedron; TET—*two adjoining tetrahedra; stressed bond-angle ranges*—$P_6(\cos\theta)$ positive.

Peaks at 60° and 109° accompanied by a broad maximum around 150° indicate a dominant tetrahedral packing. No peaks are found at 90° and 120° which proves that FCC-like local coordination can only rarely contribute. The partial average of the group ICSYS has peaks close to the bond angles of the exact icosahedron (63.5°, 116.5°, 180°). Roughly, the bond-angle distribution is similar to that which was reported for quench condensed Ca–Mg systems by Hafner (1988).

3.3. Local structure in the LDOS

The representation (11) is designed to be a suitable starting point for answering the question about the local structure properties which really enter the LDOS. According to (12), the environment correction, $\mathrm{Re}\,\Sigma_m T_{sLL}/(2l+1)$, can be decomposed into scattering paths which enter and leave the environment through atomic scattering channels $|s'L'\rangle$ and $|s''L''\rangle$, respectively. We confine our discussion to one-component systems ($f_{sl} \equiv f_l$, $\delta_{sl} \equiv \delta_l$). Thus, (9) and (2) provide

$$\exp(-\mathrm{i}2\delta_l)\sum_m T_{sLL}/(2l+1) = \sum_{\substack{s'\\ s''}}\sum_{\substack{L'\\ L''}} \frac{1}{2l+1}\sum_m G_{sL,s''L''}K_{s''L'',s'L'}G_{s'L',sL}. \tag{15}$$

Here, $K_{s''L'',s'L'}$ contains all intermediate scattering and propagation. As in the conventional diffraction theory, only in the single-scattering approximation to (15) is the influence of the atomic arrangement strictly separated from the atomic scattering. With $K_{s''L'',s'L'} \to \mathrm{i}kf_{l'}\delta_{s''s'}\delta_{L''L'}$ in (15) one arrives at

$$\sum_{l'}(2l'+1)\,\mathrm{i}kf_{l'}\sum_{\tilde{l}}(2\tilde{l}+1)S_{s\tilde{l}}\int_{-1}^{+1}\frac{\mathrm{d}x}{2}P_{\tilde{l}}P_{\tilde{l}}P_{l'} \tag{16}$$

where

$$S_{sl} \equiv \sum_{\substack{s' \\ (\neq s)}} [h_l^{(1)}(kR_{s's})]^2 \rightarrow \int \mathrm{d}^3 r \, \mathcal{N} g(r) [h_l^{(1)}(kr)]^2 \tag{17}$$

are the local structure parameters to be found ($R_{s's}$ interatomic distance, $\mathcal{N}$ average atom number density). They contain only the radial distribution of neighbours which must, thus, be the dominant structure property at the band edges where the atomic scattering is not strong. Note that the ensemble averages of the S_{sl} (17) are integral transforms of the pair correlation function $g(r)$ which include higher spherical Hankel functions. In contrast, common diffraction experiments provide only the structure factor which is the j_0 transform of $g(r)$. Hence, the LDOS is a much more sensitive probe of the local radial distribution of neighbours. With respect to the first twelve neighbours, however, the classification of the 256 atoms by the S_{sl} (17) is equivalent to that by $\bar{r}(12)$ and $\overline{\Delta r}(12)$ as employed in figure 2(*a*).

Bond angles are accounted for in (15) in the lowest order by the double-scattering contribution. It is obtained by $K_{s''L'',s'L'} \rightarrow \mathrm{i}kf_{l''}G_{s''L'',s'L'}\,\mathrm{i}kf_{l'}$ and provides $\Sigma_{s''s'}\Sigma_{mm'm''} G_{sL,s''L''}G_{s''L'',s'L'}G_{s'L',sL}$ as the structure-dependent quantities. In the following, $(s''L'')$ and $(s'L')$ will be restricted to s-scattering by the twelve nearest neighbours. Moreover, we disregard them for different distances from the central atom at $\boldsymbol{R}_s$. On such conditions, we have

$$P_{sl}(12) \equiv \frac{1}{66} \sum_{\substack{12 \\ \text{neighbours}}}^{\text{pairs}} P_l(\hat{\boldsymbol{R}}_{s''s}\hat{\boldsymbol{R}}_{s's}) \rightarrow \int_0^{\pi} \mathrm{d}\theta \, b(\theta) P_l(\cos(\theta)) \tag{18}$$

as the most simple bond-angle dependent quantities involved (P_l Legendre polynomial, $\hat{\boldsymbol{R}}_{s's}$ bond directions, $b(\theta)$ bond-angle distribution function). Steinhardt *et al* (1983) employ $Q_{sl}(12) = [(1 + 11P_{sl}(12))/12]^{1/2}$ for a 'cluster shape spectroscopy' in models of liquids and glasses. They show that nearly icosahedral first-neighbour shells are indicated by large values of $Q_{s6}(12)$. As follows from figure 2(*b*), the members of the group ICSYS occupy just the bond-angle ranges where P_6 is positive, which explains the specific behaviour of $Q_{s6}(12)$ and $P_{s6}(12)$. Upon inspecting the 256 local 13-atom clusters, we find that there is no statistical correlation between $\bar{r}(12)$ and $P_{sl}(12)$ of a cluster, except for $l = 6$ where small $\bar{r}(12)$ join only with large $P_{s6}(12)$, because the icosahedral coordination provides the most compact arrangement of 13 atoms.

4. Resonance splitting

For treating local-environment effects in the LDOS we use the frozen 256-atom equilibrium configuration which was characterized in section 3. Only the first 16 neighbours (slightly more than the first correlation shell) will be included in the calculation of the LDOS for each atom. Hence, results of this study are not qualified for quantitative comparison with photoemission spectra. A fixed number of neighbours is taken rather than all neighbours up to a fixed distance. This avoids a sharp cut-off of the environment. By the choice of 16 neighbours, any accentuation of cubical contributions (FCC-18, BCC-14) is excluded in this study. The scattering phase shifts are calculated from Herman–Skillman atomic wave functions using a local exchange–correlation potential with $\alpha = \frac{2}{3}$ and BCC-Fe as a reference structure.

4.1. The influence of the first-neighbour shell

We calculate the LDOS for the 256 local 17-atom clusters. Then, the total electronic density of states per atom is obtained upon taking the ensemble average. As shown in

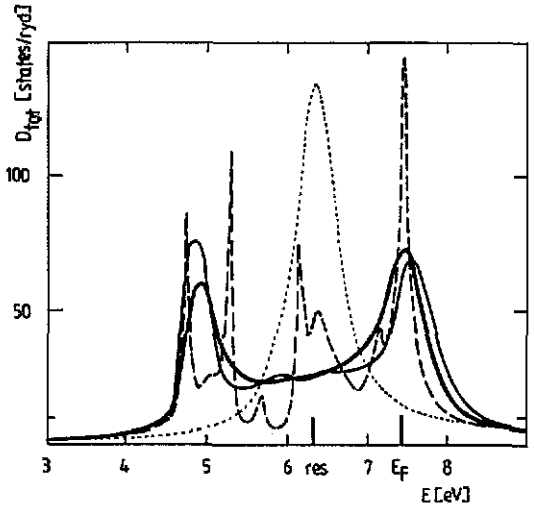

Figure 3. Total electronic density of states of an atomic sphere (model a-Fe); dotted curve—bare atomic sphere; bold full curve—ensemble average of the 17-atom clusters (E_F: Fermi energy); full curve—average of the group ICSYS; broken curve—FCC-cluster (19 atoms, distances of the first twelve neighbours from the central atom equal to the ensemble average of the 256-atom cluster); res—atomic d-resonance.

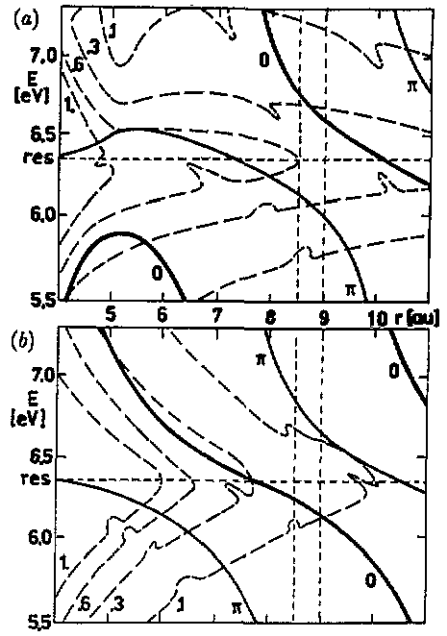

Figure 4. Contour maps of the eigenvalues β'_m of the diagonal blocks B_m (19); full curves—arg β_m, broken curves—$|\beta_m|$, res—atomic d-resonance; (*a*) $m = 0$, (*b*) $|m| = 1$. The dip of the second pair correlation shell is indicated by broken lines. Comparison with figure 2(*b*) shows that new d-states arise from MS resonances of certain axial symmetry.

figure 3, the single-peaked profile of the bare AS is split into a doublet which is well known from BCC-like coordination (Fujiwara 1984). We emphasize:

(i) the splitting consists of a distinct removal of states from the vicinity of the atomic d-resonance due to MS with neighbours in the FPCS;

(ii) bond angles have an important influence. Note that the removal of states becomes less efficient if there is a considerable content of 90° bonds to near neighbours as in the case of FCC-like coordination, figure 3. Bond angles close to 60° and 109°, however, produce distinct splittings (tetrahedral or icosahedral coordinations, figures 2(*b*), 3).

(iii) We will show that the trend for band splitting is due to d-resonance splitting by electronic MS between the effective atom considered and the single close neighbours of it.

4.2. LDOS modification due to one-neighbour cycles

Again, we employ the decomposition concept (12) and calculate a partial environment correction for d-states in (11) omitting all cycles but those with a certain neighbour (index n) which is placed on the polar axis. Hence, no transitions in the polar projection m of the angular momentum can occur. The matrix $C_{sn}C_{ns} \equiv B$ of the scattering-path cycle s–n–s is block-diagonal (diagonal blocks B_m with B_m and B_{-m} degenerate). With (9) and (2) we obtain this partial environment correction due to cycles with only one neighbour as the real part of the complex quantity

$$T_2 \equiv \frac{\exp(i2\delta_2)}{ikf_2}\frac{1}{5}\sum_{m=-2}^{2}[(I - B_m)^{-1}B_m]_{22}. \tag{19}$$

It is interesting to see, for our effective Fe atoms, how T_2 behaves in the energy range of the valence states for pair distances up to next-nearest neighbours. Figure 1(b) shows contour maps of $|T_2|$ and arg T_2 based on a given net of distances and energies. Upon applying the statement at the end of section 2.2 we conclude: MS with neighbours in the FPCS removes electronic d-states at energies close to the atomic d-resonance (arg $T_2 \approx \pi$, figure 1(b)). About 1 eV below and above, however, d-states are piled up (arg $T_2 \approx 0$), in particular with neighbours on the core side of the FPCS, due to large values of $|T_2|$. Hence, the atomic d-resonance splits into two components.

According to (19), MS effects in T_2 can be attributed to eigenvalues β_m of certain diagonal blocks B_m. It turns out that, at best, one eigenvalue in each diagonal block has $(1 - \beta_m)^{-1}$ large enough to make essential contributions to T_2, i.e. arg β_m close to 0 together with $|\beta_m|$ not much less in comparison to 1. As shown in figure 4(a), for this active eigenvalue β_0, the condition arg $\beta_0 \approx 0$ is fulfilled just in the energy–distance region where, in figure 1(b), the emergence of the bonding doublet component is indicated by arg $T_2 \approx 0$. In the same region, there is rather destructive interference in diagonal blocks with $|m| = 1$ as follows from arg β_1 close to π (figure 4(b)). The bonding component of the doublet is thus generated by an MS resonance in a pair of effective atoms, where $m = 0$ is the axial projection of the angular momentum. This gives rise to (let us call it) the σ-resonance. Similar arguments apply to the antibonding doublet component and β_1 (figures 4(b), 1(b)). Hence, it will be referred to as the π-resonances ($|m| = 1$). There are less important effects in β_2 at smaller interatomic distances which do not occur in the structure model.

4.3. Coupling of adjoining pair effects

According to (12) and (9), the individual pair processes between a central atom and its neighbours are linked by cycles which include at least two neighbours. The axial symmetry that gives rise to separate σ- and π-resonances in a pair of effective atoms is broken with the consequence that σ- and π-resonances of all adjoining pairs are mixed. For simplicity we confine the discussion (i) to links at the central atom itself and (ii) to neighbours which belong to the FPCS. On such conditions, only the σ–σ coupling and the π–π coupling can be efficient. Because, as follows from figure 4, at most, one of both pair resonances is tuned to constructive interference which makes σ–π coupling generally inefficient.

Due to the isotropy, the s-scattering at the central atom is very important with respect to the coupling of adjoining pair resonances. However, s-scattering participates only in σ-resonances ($m = 0$) which are destined for structure-induced modification or even decay.

Two separate peaks are seen in the total density of states per atom in figure 3 where linked pair effects with 16 neighbours are included. It can be guessed that the pair-like resonance splitting is preserved despite the coupling. In that case, the bonding (antibonding) peak should be due to the σ-(π-)resonances of the adjoining pairs. For a decision, we calculate the d-LDOS for a typical member (ICOCL) of the group ICSYS, first including s-scattering and then without it (figure 5). Only the bonding peak is modified upon omitting the s-scattering which has almost the same strength throughout the d-band. We conclude that σ-resonances do not contribute to the antibonding peak in figure 3. This peak is really due to π-resonances ($|m| = 1$) in adjoining atom pairs. A similar

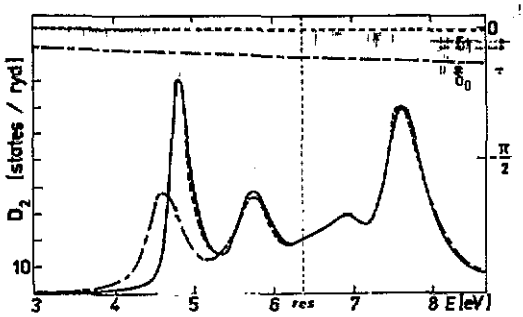

Figure 5. The antibonding peak of d-states is not influenced by σ-resonances as demonstrated for the ICOCL (20 neighbours considered); full curve—including δ_0, δ_1 and δ_2; chain curve—including δ_1 and δ_2; broken curve—including δ_0 and δ_2.

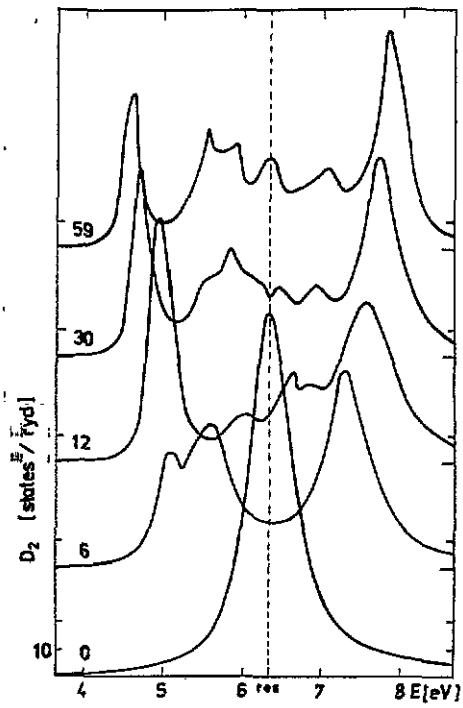

Figure 6. The d-DOS of the ICOCL with 0, 6, 12, 30, 59 neighbours considered. The bounding peak appears most pronounced with twelve neighbours. σ-resonances tend to decay upon coupling.

direct test with respect to the bonding peak and σ-resonances is not available. However, as pointed out above, σ–π coupling is less efficient. Note, in addition, that the very weak p-scattering can be omitted without consequences (figure 5).

Are there really two peaks in the LDOS of amorphous Fe? In view of figure 3 we ask for possible peak extinctions upon including more than 16 neighbours in each local cluster. The following items seem to be essential.

(i) 25% of the 256 local d-bands exhibit additional structure in the bonding peak but none in the antibonding one. This confirms the structure sensitivity of the σ-resonances.

(ii) Trends to be seen in the d-LDOS of the ICOCL upon extending the included environment help to estimate if the bonding peak can survive in amorphous Fe with a high content of dense centres.

Figure 6 shows the d-LDOS with a growing number of neighbours considered ((six on the core side of the FPCS, 12 complete the almost icosahedral shell, 30 (59) include the first (second) subpeak of the SPCS). The bonding peak appears most pronounced at twelve neighbours. Then, coupling to the SPCS, makes it decrease in favour of the monotonously rising antibonding peak. This is supported by intervening curves which are not displayed. Note that no hint of saturation is found upon completing the SPCS.

We conclude that mainly the bonding peak (coupled σ-resonances) is destroyed by long-range MS. This goes down to a sequence of narrow lances in BCC-Fe (Singh *et al* 1975) or to a weak shoulder in liquid and amorphous phases. The bonding peak is generated by local effects; its extinction, however, requires MS of s-waves to be considered well beyond the SPCS. The main peak of UPS spectra (Pessa *et al* 1976, Paul and

Neddermeyer 1985) results from moderately interacting π-resonances. Thus, resonance splitting by intra-pair MS and inter-pair coupling of σ-resonances are essential for the structure-LDOS connection in a non-crystalline transition metal.

5. Towards the splitting of the SPCS

The splitting of the SPCS reflects certain geometric arrangements of next-nearest neighbours which predominate statistically against thermal fluctuations owing to enhanced attractive interatomic forces. We have demonstrated in section 3 that additional inward-pointing forces, even in the dip of the SPCS, produce a distinct and realistic splitting. Here, we will discuss if MS in a pair of effective Fe atoms can explain attractive forces beyond $1.4\,r_0$.

In the following discussion, we take the energy in the vicinity of the atomic d-resonance. In figure 1(b), for neighbours in the dip (the subpeaks) of the SPCS, we find $\arg T_2 \approx \pi(0)$. This indicates that a decrease (an increase) of the d-LDOS at the central atom will arise from MS with such partners. Hence, upon splitting the SPCS, d-states can be generated close to the atomic d-resonance and thus below the Fermi energy (figure 3). This may reduce the electronic contribution to the total energy and will be realized in that case. Due to increasing $|T_2|$ at decreasing interatomic distance (figure 1(b)), it is more efficient to populate the first subpeak than the second one. From figure 4 it follows that π-(σ-)resonances are excited along the bonds to neighbours in the first (second) subpeak of the SPCS. For neighbours in the dip, however, $(\pi/2)$-passages of $\arg \beta_0$ and $\arg \beta_1$ indicate indifferent interference states of both resonances. The Jahn–Teller effect of molecules and solids (see Sturge 1967) shows how complex systems respond to frustrating competition of electronic states with different symmetries: the ions are moved into positions where the system is more tightly bound without electronic degeneracy. In the present case, the σ–π frustration can be removed by forces which push the neighbours in the dip towards one of the subpeaks of the SPCS where one of both resonances is tuned to constructive interference. Around each Fe atom, between the subpeaks of the SPCS, there should be an energetic drawback for other Fe atoms to be located there. Even BCC-Fe has no neighbour shell right in the dip region (figure 1(a)).

Very recently, H–NFE–TB results were reported for the effective interatomic potential of liquid Fe (Hausleitner *et al* 1991). At distances which belong to the SPCS, a weak potential peak is generated by the simple-metal contribution. We show that d-electrons, owing to the effective-atom d-resonance splitting, may also act in this way.

6. Local electronic density of states and the radial distribution of neighbours

It has been previously emphasized that the LDOS of liquid and amorphous metals largely depends on the radial distribution of neighbours (Khanna and Cyrot-Lackmann 1980, Cyrot-Lackmann 1984). Several papers have dealt with the electronic consequences of passing over from the liquid to the amorphous state (Fujiwara 1979, Khanna and Cyrot-Lackmann 1980, Krajči 1987). Unfortunately, the approach employed in the LDOS has a greater influence on the results.

As pointed out in section 4, the doublet of d-states is mainly due to MS with neighbours in the FPCS. Close to the atomic d-resonance, there are states which are derived from MS with neighbours in the SPCS (section 5). The edges of the d-LDOS lie about 2 eV below

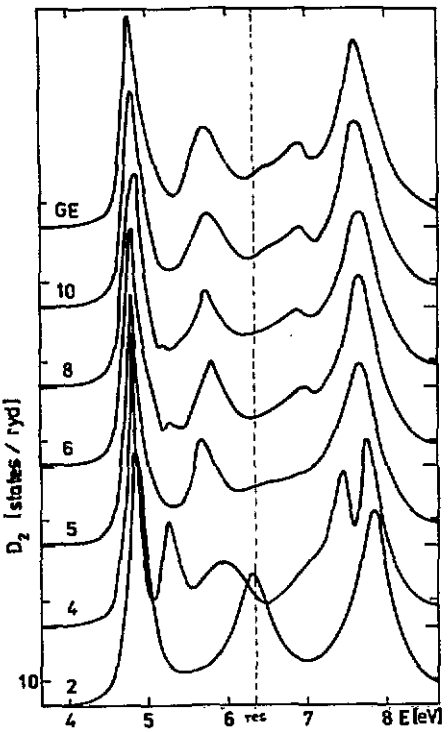

Figure 7. The d-DOS of the ICOCL (20 neighbours considered) calculated by the scattering-recursion method upon terminating the continued fraction (13) after 2, 4, 5, 6, 8, 10 recursion steps; GE—Gaussian elimination. At the d-band edges dominate scattering paths with many returns to the central atom which are considered by a few recursion steps.

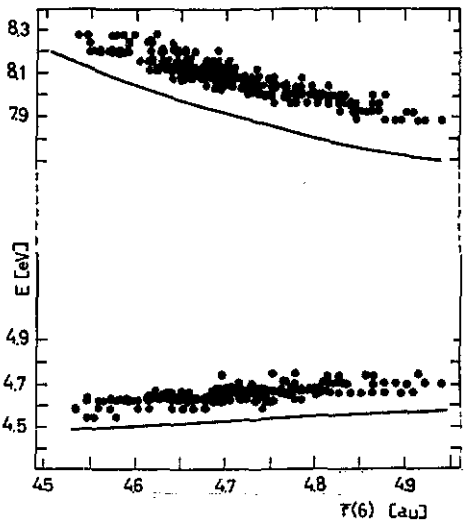

Figure 8. Energy positions of the upper (top) and the lower (bottom) 15-states Ryd^{-1} levels of the 256 local d-bands plotted versus the average distance of the first six neighbours, $\bar{r}(6)$. For comparison, curves of constant arg T_2 (cf figure 1(*b*)). MS in very close pairs dominates at the d-band edges.

(above) the atomic d-resonance where the σ-(π-)resonances with first neighbours are weakly excited. In order to produce a net effect, they have to be coupled most constructively, which is accomplished with links at the central atom itself. Such scattering paths are fully included after two recursion steps of the scattering recursion method (section 2). On this level of the continued fraction (13), all possible arrangements of elementary loops $\langle sL|C^n|sL\rangle$ are included up to $n = 4$. Hence, the positions of the d-band edges should be obtained almost accurately. This is proved for the ICOCL in figure 7. Results are taken from several levels of the continued fraction and compared with Gaussian elimination. Note that at least five recursion steps are needed to remove chaotic peaks in the vicinity of the atomic d-resonance.

At the d-band edges, scattering paths with many returns to the central atom dominate. Such MS must be highly sensitive to the radial distribution of neighbours. For each local 17-atom cluster, we have obtained the energies where the d-LDOS passes through 15 states Ryd^{-1} (level of the lower point of inflexion in the density of d-states per atom). As shown in figure 8, there is obvious correlation with the average distance, $\bar{r}(6)$, of the first six neighbours. Six neighbours form roughly the core side of the FPCS. Our concept of dominant pair processes at the d-band edges is supported by the fact that the points in figure 8 are arranged along curves arg T_2 = constant (see figure 1(*b*)). The upper edge is more sensitive to $\bar{r}(6)$ than the lower one. Note the enhanced fluctuation of the upper

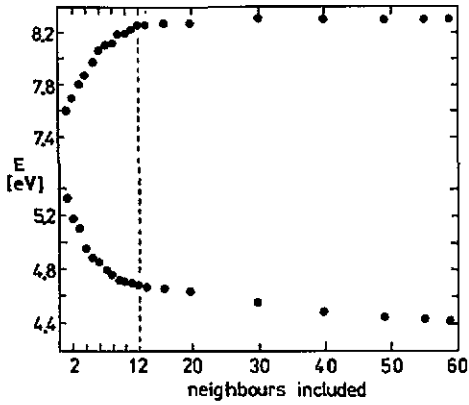

Figure 9. Energy positions of the upper (top) and the lower (bottom) 15-states Ryd^{-1} levels of ICOCL with up to 59 neighbours considered. The upper d-band edge depends only on the short-range order. The lower edge is influenced by long-range MS.

edge, which indicates that besides $\bar{r}(6)$, other structure properties may also act in a systematic manner. The bond angles between the first six neighbours can be excluded in this respect, because representations like figure 8 with $\bar{r}(6)$ replaced by $P_{sl}(6)$ (18) with $l = 1, \ldots, 5, 7, \ldots, 10$ do not show the given positions of the upper edge well distributed along lines.

Differences in the density of states per atom of liquid and amorphous transition metals which are due to different shapes of the core side of the FPCS are thus to be found above the Fermi level (see figure 3). They should be obtained by inverse photoemission rather than by photoemission.

These conclusions are drawn from a small-cluster study (17-atom clusters). In order to prove the reliability we have obtained the d-band edges for the ICOCL including up to 59 neighbours with all possible channel-to-channel links. This goes beyond the SPCS (see figure 1(*a*)). As shown in figure 9, the upper edge stays almost unmoved after completing the FPCS; it is only sensitive to the short-range order. The lower edge, however, continues moving downwards where the bonding peak decreases in favour of the antibonding peak (cf figure 6). No trend for saturation is seen in this process.

7. Conclusions

Within a muffin-tin model for a dense-packed metallic material, the LDOS of an atomic sphere is derived from the bare-atomic sphere LDOS and complex amplitudes of the L-diagonal back-scattering of spherical waves by the environment. This representation provides direct access to the interplay between the LDOS and the real-space structure. We show that integral transforms of both the pair correlation function and the distribution of bond angles to nearest neighbours are the most simple structure properties that enter the electronic density of states per atom in the single and double scattering approximation, respectively.

Pure amorphous Fe is used as a model of amorphous transition metals. We show that electronic MS in a pair of effective atoms has fundamental importance for valence electrons in such materials. The following conclusions can be drawn.

(i) A trend towards a double peak of d-states is set by separate MS with each neighbour on the core side of the FPCS upon d-resonance splitting. MS with the FPCS as a whole acts in the same way, at least for nearly tetrahedral or icosahedral coordination. MS with the more distant environment removes the bonding component of the resonance doublet where s-scattering plays an essential part in this process.

(ii) The dominant structure property at the upper band edge is the radial distribution of the neighbours on the core side of the FPCS. For energies in the vicinity of the atomic d-resonance, however, the bond-angle distribution is very important. Medium- and long-range order forms the lowest part of the band.

(iii) MS with neighbours in the SPCS indicates that the neighbours in the dip between the two subpeaks are in disadvantageous positions. Upon moving them towards one of the subpeaks, the electronic energy can be lowered and a frustrating equivalence of MS resonances with different axial symmetries is removed. Similar to the Jahn–Teller effect, this should be accomplished by a corresponding part of the effective interatomic force which pushes the atoms in the dip towards the subpeaks.

Acknowledgments

We wish to thank Professor R Lenk for stimulating discussions and his permanent interest in the progress of this work and Professor P Ziesche who drew the attention of one of us (HS) to similarities with the Jahn–Teller effect.

Appendix

Basic solutions of the angular momentum $L = (l, m)$:

$$\varphi_L(\boldsymbol{r}) \equiv \mathrm{i}^l \varphi_l(kr)\sqrt{4\pi}Y_L(\hat{\boldsymbol{r}}).$$

Radial part $\varphi_l(z)$ outside the MT sphere:

$$J_{sl}(z) = j_l(z)\cos(\delta_{sl}) - n_l(z)\sin(\delta_{sl}) = \exp(-\mathrm{i}\delta_{sl})(j_l(z) + \mathrm{i}kf_{sl}h_l^{(1)}(z))$$

$$H_{sl}^{+}(z) = \exp(\mathrm{i}\delta_{sl})h_l^{(1)}(z).$$

($j_l(z)$, $n_l(z)$ and $h_l^{(1)}(z) \simeq \mathrm{i}^{-1}\exp(\mathrm{i}z)/\mathrm{i}z$ are spherical Bessel functions of the first, the second and the third kind, respectively.)

Spherical harmonics:

$$Y_{l,m}(\hat{\boldsymbol{e}}) = (-1)^{(|m|-m)/2}\left[\frac{(2l+1)(l-|m|)!}{4\pi(l+|m|)!}\right]^{1/2}\frac{\mathrm{d}^{|m|}}{\mathrm{d}t^{|m|}}P_l(t)|_{t=e_z}(e_x + \mathrm{i}\,\mathrm{sgn}(m)e_y)^{|m|}.$$

Bare-atomic sphere electronic density of states:

$$D_{sl}^{0}(E) = -(k/\pi)(2l+1)\{[rJ_{sl}(kr)]^2\,\mathrm{d}(\Gamma_{sl}(kr))/\mathrm{d}E\}|_{r=\mathrm{ASs}}$$

where Γ_{sl} are logarithmic derivatives.

References

Ballentine L E and Kolář M 1986 *J. Phys. C: Solid State Phys.* **19** 981
Bennett C H 1972 *J. Appl. Phys.* **43** 2727
Cargill G S 1975 *Solid State Physics* vol 30 (New York: Academic) p 227
Cyrot-Lackmann F 1984 *J. Non-Cryst. Solids* **61–62** 1027
Fujiwara T 1979 *J. Phys. F: Met. Phys.* **9** 2011
—— 1984 *J. Non-Cryst. Solids* **61–62** 1039
Fujiwara T and Ishii Y 1980 *J. Phys. F: Met. Phys.* **10** 1901

Gonis A, Zhang X-G and Nicholson D M 1989 *Phys. Rev.* B **40** 947
Gyōrffy B L and Stott M J 1971 *Solid State Commun.* **9** 613
Hafner J 1988 *J. Phys. F: Met. Phys.* **18** 153
Hafner J and Jaswal S S 1988 *J. Phys. F: Met. Phys.* **18** L1
Harris R and McMaster B N 1986 *J. Phys. C: Solid State Phys.* **19** 7217
Hausleitner Ch, Kahl G and Hafner J 1991 *J. Phys.: Condens. Matter* **3** 1509
Häussler P 1991 *Glassy Metals III (Springer Topics in Applied Physics)* ed H Beck, H-J Güntherodt (Berlin: Springer) at press
Haydock R, Heine V and Kelly M J 1972 *J. Phys. C: Solid State Phys.* **5** 2845
—— 1975 *J. Phys. C: Solid State Phys.* **8** 2591
Haydock R and Kelly M J 1975 *J. Phys. C: Solid State Phys.* **8** L290
Heine V 1967 *Phys. Rev.* **153** 673
Hilsch R 1960 *Non-Crystalline Solids* ed V D Frechette (New York: Wiley)
Ichikawa T 1973 *Phys. Status Solidi* a **19** 707
Jones H 1973 *Rep. Prog. Phys.* **36** 1425
Khanna S N and Cyrot-Lackmann F 1980 *Phys. Rev.* B **21** 1412
Krajči M 1987 *J. Phys. F: Met. Phys.* **17** 2217
Krajči M and Mrafko P 1988 *J. Phys. F: Met. Phys.* **18** 2137
Ley L, Dabbrousi O B, Kowalczyk S P, McFeely F R and Shirley D A 1977 *Phys. Rev.* B **16** 5372
Li Jin-Chen and Cowlam N 1990 *J. Non-Cryst. Solids* **117/118** 148
Mattheiss L F 1964 *Phys. Rev.* **134** 192
Milstein F 1973 *J. Appl. Phys.* **44** 3825
Nex C M M 1978 *J. Phys. A: Math. Gen.* **11** 653
Nold E, Lamparter P, Olbrich H, Rainer-Harbach G and Steeb S 1981 *Z. Naturforsch.* **36a** 1032
Paul Th and Neddermeyer H 1985 *J. Phys. F: Met. Phys.* **15** 79
Pessa M, Heimann P and Neddermeyer H 1976 *Phys. Rev.* B **14** 3486
Sadoc J F, Dixmier J and Guinier A J 1973 *J. Non-Cryst. Solids* **12** 46
Singh M, Wang C S and Callaway J 1975 *Phys. Rev.* B **11** 287
Solbrig H 1987 *Phys. Status Solidi* b **139** 223
Steinhardt P J, Nelson D R and Ronchetti M 1983 *Phys. Rev.* B **28** 784
Sturge M D 1967 *Solid State Physics* vol 20 (New York: Academic) p 91
Varga S and Krempasky J 1989 *J. Phys.: Condens. Matter* **1** 7851
Varga S 1990 *J. Phys.: Condens. Matter* **2** 8303
Verlet L 1967 *Phys. Rev.* **159** 98
Watanabe M S and Tsumuraya K I 1990 *J. Non-Cryst. Solids* **117/118** 187
Ziman J M 1965 *Proc. Phys. Soc.* **86** 337